Tracking Studies for the Upgrade II of the LHCb Experiment

This work has been carried out by

Penelope Hoffmann

CERN, Heidelberg University (DE)

under the supervision of

Dr. Renato Quagliani

and

Dr. Alessandro Scarabotto

September 2024

Abstract

Improving physics studies at LHCb through increased statistics necessitates a major upgrade of the LHCb detector, to be installed at the beginning of Long Shutdown 4. The Upgrade II detector will operate at luminosities of up to $1.5 \times 10^{34}\,\mathrm{cm}^{-2}\,\mathrm{s}^{-1}$, a 7.5 times higher luminosity than the Upgrade I detector. As part of the upgraded detector, a new hybrid tracker, the Mighty Tracker (MT), consisting mainly of scintillating fibres and high-granularity pixels in the high-occupancy region will replace the Scintillating Fibre tracker (SciFi) placed downstream of the LHCb dipole magnet.

The work presented here studies the effect of the detector layout on the performance of the tracking system. Particular focus will be given to the design and performance of the stand-alone track reconstruction algorithm for those tracks which are expected to pass through the downstream tracker in both the pixel and fibre acceptance. The tracks found by this algorithm are the seeds to reconstruct the tracks passing through the full LHCb spectrometer as well as the daughters of long-lived particles such as K_s and Λ which do not leave any signature in the Vertex Locator of the LHCb detector.

Contents

1 Introduction

For improving the precision of physics analysis at LHCb through higher statistics, an increase in luminosity up to $1.5 \times 10^{34}\,\mathrm{cm}^{-2}\,\mathrm{s}^{-1}$, a factor of 7.5 with respect to Run 3, is proposed for Run 5. However, this increase in luminosity poses new challenges for the detector and the tracking system, as it has to cope with high data rates, high occupancies, and high radiation doses which cannot be handled by the current detector setup. This outlines the need for the proposed Upgrade II detector [1], and thus also new tracking algorithms tuned to the detector layout, as a robust tracking and reconstruction performance is crucial for physics analysis. A key part of the tracking system, as most physics analyses use tracks with hits in this detector, is the Mighty Tracker (MT), which is a new hybrid tracker consisting of scintillating fibers as well as high-granularity pixels covering the high-occupancy region that is set to replace the current downstream tracker.

The first part of this work is focused on studies of the momentum resolution of different track types for varying tracking sub-detector setups. In Section 3.2, different scenarios of material placement in the tracker before the magnet and their effect on the momentum resolution of tracks traversing the whole spectrometer are studied, while in Section 3.3, the effect of shifting the first pixel layer of the MT towards the magnet on the momentum resolution for different track types is investigated.

The central part of this work is dedicated to the track reconstruction performance for tracks reconstructed solely from hits in the downstream tracker. These tracks can be used as seeds for tracks passing through the whole LHCb detector as well as for the search for long-lived particles. Here, the main focus is put on the adaptation of the reconstruction algorithm for tracks that traversed both the pixel and fiber acceptance of the MT. The design of the algorithm is described in Section 4.5 and the performance is evaluated in Section 4.6.

Lastly, the previously reconstructed tracks in the MT are used as seeds to reconstruct tracks leaving hits in every tracking detector, via an algorithm known as "matching". Preliminary studies on the performance of this algorithm as well as possible points for improvement are presented in Section 5.

2 The Tracking System in Upgrade II

The main purpose of the tracking system is to measure the electromagnetic interaction of particles with the detector material to reconstruct the tracks of these particles. It aims to provide excellent vertex resolution and a good momentum resolution of 0.4-$0.5\,\%$. The layout of the tracking system in the Upgrade II of the LHCb detector is shown in Figure 1. Additionally, the varying track types reconstructed at LHCb are illustrated.

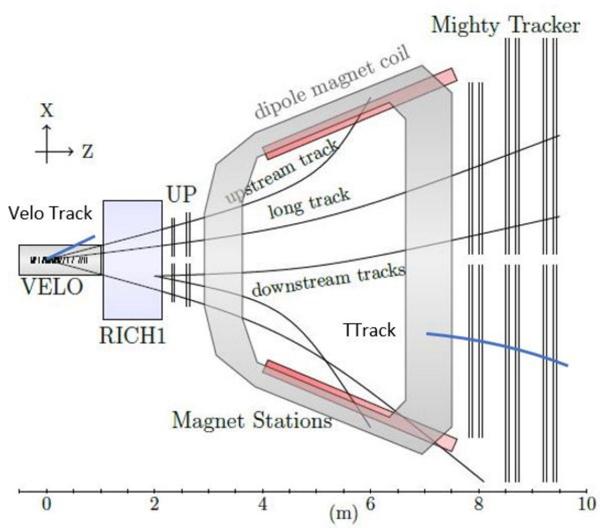

Figure 1: Sketch of the proposed tracking detector layout and the different track types at LHCb. Adapted from [1].

Long Tracks: These tracks traverse the full spectrometer leaving hits in the Vertex Locator (VELO), Upstream Pixel Tracker (UP), and Mighty Tracker (MT). They have the highest momentum resolution and are thus essential for physics analysis. However, only VELO and MT hits are required for tracks to be reconstructable.

Upstream Tracks: Upstream Tracks are low momentum tracks that are bent out of acceptance by the magnetic field. For reconstruction, hits in the VELO, the UP, and the Magnet Stations are utilized.

Downstream Tracks: Decays of long-lived particles can result in tracks with only hits in the UP and the MT.

VELO Tracks: Velo Tracks are reconstructed solely from hits in the VELO. They are used as seeds for long and upstream tracks as well as for primary vertexing (pp colli-

sions) and secondary vertexing (decays of b or c hadrons).
TTracks: TTracks are composed of hits found in the MT and can be used as seeds for both long and downstream tracks.

2.1 Vertex Locator

In light of the increased luminosity for Upgrade II, the Vertex Locator (VELO) faces significant challenges concerning the efficient and precise reconstruction of all primary and secondary vertices in the instrumented acceptance of $2 < \eta < 4.8$. Due to an estimated pile-up, e.g. the average number of pp collisions per beam-beam crossing, of ~ 40, the detector has to cope with large particle multiplicities and data rates as well as a high, non-uniformly distributed radiation dose. Thus, in order to handle the increased radiation dose and data rates, the minimal distance between the interaction point and the detector elements will be increased from $5.2\,\mathrm{mm}$ in Upgrade I to $7.2\,\mathrm{mm}$ and the pixel pitch is planned to be 55x$55\,\mu\mathrm{m}^2$. However, a significant reduction in the material budget of the VELO is required to maintain a similar impact parameter resolution to Upgrade 1. This is achieved by reducing the material of the RF foil that separates the secondary detector vacuum from the LHC vacuum. For facilitating track reconstruction and vertexing, the addition of timing information to the detector is crucial. Each hit should have a time resolution of $50\,\mathrm{ps}$ leading to an overall track time resolution in the range of $20\,\mathrm{ps}$. To reconstruct a track in the VELO, a particle should cross five detector stations and leave a minimum of three hits.

2.2 Upstream Pixel Tracker

The Upstream Pixel Tracker (UP) as the second tracking detector is located directly before the magnet and thus experiences the fringe field of the dipole magnet. The inclusion of the UP serves to improve the momentum resolution of tracks and to reduce the rate of incorrect matching between VELO and TTracks. In order for the performance of the UP to not be drastically impacted by the higher occupancy, it is planned to change from silicon strip to silicon pixel technology. With an estimated pitch of 50x$150\,\mu\mathrm{m}^2$ and therefore the precise measurement of information in y direction, stand-alone track reconstruction is possible for the first time. Due to the proximity to the magnetic field and the significant negative impact of multiple scattering on track reconstruction and momentum resolution in this region, the overall material budget of the detector has to be reduced as far as possible. An overall material budget of $\sim 6\,\%$ is aimed for.

2.3 Mighty Tracker

The Mighty Tracker is the last and largest detector dedicated to track reconstruction and is located downstream of the magnet. Therefore, it plays a crucial role in track reconstruction and in providing a precise track momentum estimate together with the Velo and the UP. Since the high particle flux and consequently induced radiation damage as well as the high occupancy in Upgrade II conditions would lead to a serious degradation in performance when running with the Upgrade I setup, the installation of a hybrid tracker consisting of the Fibre Tracker (FT) and the Mighty Pixel (MP) is planned.

Similar to the Upgrade I detector layout, the Fibre Tracker is designed as a scintillating fibre tracker with 12 detection layers spread over three stations. In every station, the first and last fibre mats are oriented vertically, while the two stereo layers are rotated by $\pm 5^{\circ}$ (x-u-v-x layout) to allow for the measurement of the y component of a track.

The Mighty Pixel, as a high-granularity silicon pixel system, replaces the scintillating fibres in the high occupancy region. It consists of six layers, 2 detection layers per station, mounted at the same z position, where the x layers of the FT are located. The area instrumented by pixels is removed from all 12 FT layers and the pixels have a hole of $260\text{x}260\,\mu\text{m}^2$ to leave space for the beam pipe. With a pitch size of $50\text{x}150\,\mu\text{m}^2$, the pixels have similar specifications as the ones in the UP. While the driving factors for installing a pixel detector are the increased radiation hardness and better performance at high occupancies, it also has advantages in the track reconstruction as it provides precise measurements in the y direction.

2.3.1 Geometry Options

Four different MT geometries (Baseline, Low, Medium, High) are taken into consideration while carrying out the tracking performance studies. The geometries differ solely in the form and size of the area that is instrumented with pixels. The total area each scenario covers is documented in Table 1 and a visualization of the different geometries is given in Figure 2. The final chosen pixel geometry will need to satisfy cost, occupancy, and performance considerations.

Table 1: Overall area covered by pixels for all four studied MP geometries.

Geometry	Baseline	Low	Medium	High
Area [m^2]	18	8	13	13

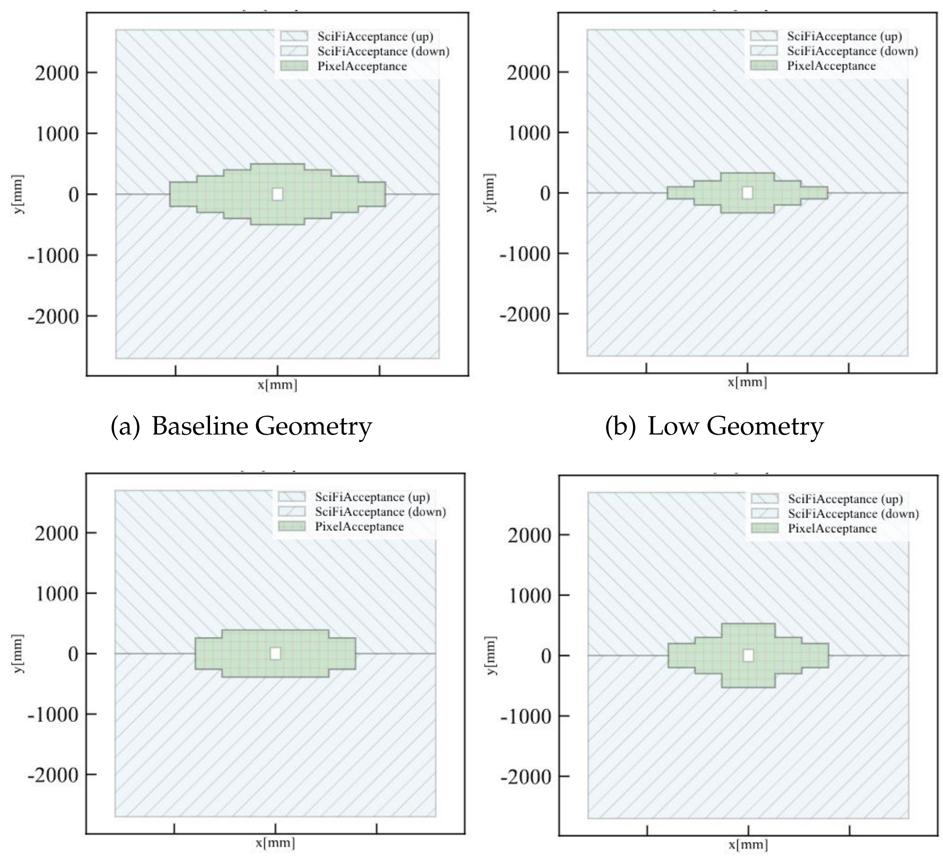

(a) Baseline Geometry

(b) Low Geometry

(c) Medium Geometry

(d) High Geometry

Figure 2: The four studied MT detector geometries: Baseline (upper left), Low (upper right), Medium (lower left), High (lower right).

2.3.2 Setups

In the longitudinal plane, the tracking performance of two different setups will be tested. For the first setup, the pixel layers are mounted in the same plane as the fibre x layers (compare Figure 3(a)). Here, fibre and pixel layers share the same z position. The setup is denoted as the "default" setup since the studied track reconstruction algorithms were implemented and tuned taking this layout into account. However, due to mechanical constraints, this layout is not realistic. Therefore, a second setup, the "shifted" setup, in which the pixel layers are shifted out of the fibre layers (see Figure 3(b)) is introduced. Different shifts of the first pixel layer will be studied regarding the impact on the tracking performance.

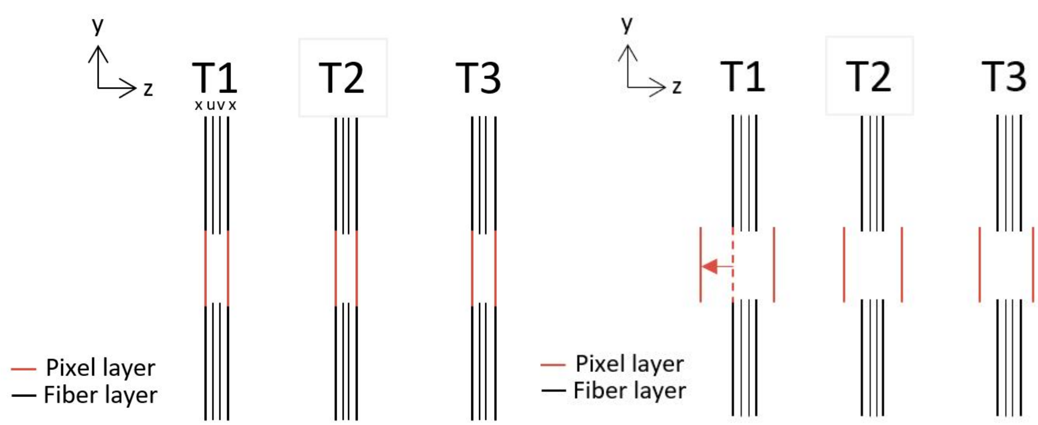

(a) "Default" setup (b) "Shifted" setup

Figure 3: Sketch of the "default" (left) and the "shifted" (right) setup for the MT.

3 Momentum Resolution Studies

The precise determination of the momentum of a track is crucial for performing physics analysis as the momentum resolution influences important quantities, such as the mass of particles and decay-time dependent observables. Hence, studies on the momentum resolution varying the material budget and the geometry of the UP and MT, respectively, were carried out using a dedicated offline framework.

3.1 Weight Matrix Formalism Framework

This framework, based on the weight matrix formalism (detailed description in [2],[3]), allows the flexible study of the effect of different detector configurations on the momentum resolution, as it does not require simulations to run over. Instead, only track kinematics from a toy sample are needed. The momentum resolution is calculated using a principle similar to a Kalman Filter applied in the uncertainty space. The parametrically determined covariance matrix of the track states is propagated along the measurement planes and noise from multiple scattering, modeled according to the material budget of the planes, is added. The resolution is then obtained by inverting the weight matrix after the propagation over all measurements. Both forward and backward propagation are possible, allowing for the study of the momentum resolution for different track types. The following studies are carried out using the kaon track kinematics from a $B^{\pm} \to K^{\pm}\mu^{+}\mu^{-}$ toy sample as well as Run 5 detector configurations, where adjustments to the material budget for different detector parts are possible.

3.2 UP Material Placement Studies

The objective of this study is to evaluate the effect of material placement in the Upstream Pixel Tracker on the momentum resolution for long tracks. To achieve this, three different scenarios of repartitioning the material are considered and the respective momentum resolutions are compared to the Run 3 baseline configuration results.
The scenario denoted *Equal distribution* refers to the overall material budget being distributed evenly across the four pixel layers and the two cooling boxes, placed at the entrance and the exit of the UP, respectively. In the *Entrance* scenario, the material is largely placed in the cooling box at the beginning of the UP and the first pixel layer,

while the remaining pixel layers and cooling box only contribute minimally to the overall material budget. Conversely, in the *Exit* scenario, only the last pixel layer and the cooling box at the exit of the UP are assigned significant material budgets.

Table 2: Material budget distribution in the UP dependent on the studied scenario.

	Material x/x_0			
Layer	Equal distrib.	Entrance	Exit	Run 3
Cooling Box (Entrance)	$1\,\%$	$4.8\,\%$	$0.1\,\%$	$0.83\,\%$
UT layer 1	$2\,\%$	$4.8\,\%$	$0.1\,\%$	$2\,\%$
UT layer 2	$2\,\%$	$0.1\,\%$	$0.1\,\%$	$2\,\%$
UT layer 3	$2\,\%$	$0.1\,\%$	$0.1\,\%$	$2\,\%$
UT layer 4	$2\,\%$	$0.1\,\%$	$4.8\,\%$	$2\,\%$
Cooling Box (Exit)	$1\,\%$	$0.1\,\%$	$4.8\,\%$	$0.83\,\%$

For all scenarios running with the Run 5 configuration, the overall material budget of the UP is fixed to $10\,\%$, and a toy sample of 10k events is simulated within the weight matrix formalism framework. The specific material budget configurations for each scenario as well as the Run 3 baseline are listed in Table 2.

The performance for each scenario in terms of the momentum resolution of long tracks is shown in Figure 4. For ease of comparison to the Run 3 baseline, the momentum resolutions are calculated for long tracks with solely fibre hits in the Mighty Tracker. The discrepancies in the resulting momentum resolution distributions for the baseline and the equal distribution scenario can attributed to the differences in the downstream acceptance covered by fibres due to the change in the detector setup. This is also reflected in the underlying histograms for the Run 3 (black) and Run 5 (red) configurations as the Run 5 histogram has fewer entries in the high momenta region.

Comparing the momentum resolutions for each scenario in terms of both momentum and transverse momentum, similar behaviour in regard to the different scenarios is observed. The entrance scenario consistently outperforms all other scenarios, while the exit scenario performs worst out of all three scenarios and for low momenta performs even worse than the Run 3 baseline. Thus, the optimization, e.g. minimization, of the material budget at the exit of the UP might lead to a significant improvement in the momentum resolution for long tracks.

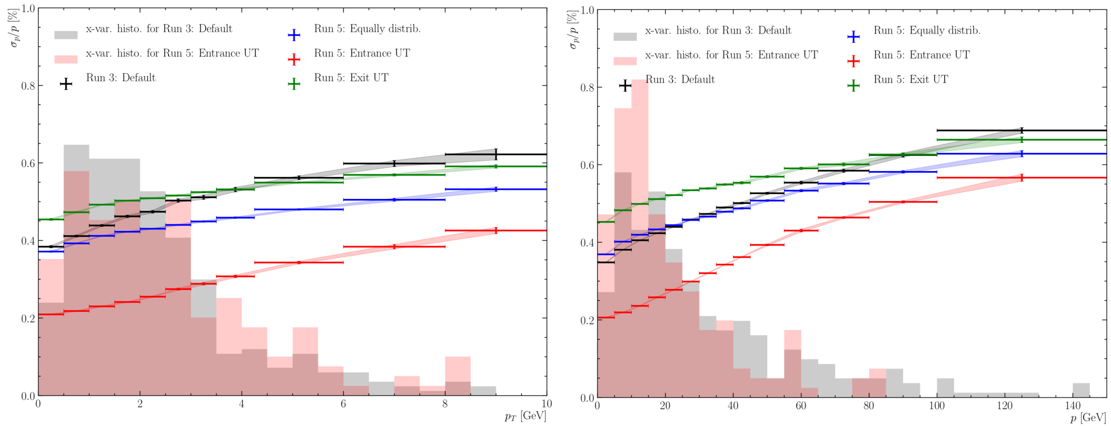

(a) Momentum resolution vs. transverse momentum

(b) Momentum resolution vs. momentum

Figure 4: Comparison of long track momentum resolution for UP material placement scenarios as a function of kinematic variables. The momentum resolution is displayed for long tracks with hits in the fibre part of the Mighty Tracker.

3.3 MP Placement Studies

The aim of this study is the cross-validation of the results from a previous study [4] regarding the impact of a potential shift of the first Mighty Pixel layer towards the magnet on the momentum resolution for different track types. These results were obtained by running over a modified Run 3 simulation, in which only the pixel layer without any surrounding services (cables, cooling, frames) was shifted. With larger shifts of the pixel layer in the upstream direction, a sizeable improvement in the momentum resolution for TTracks and a small improvement for long tracks was determined.

For the cross-validation study, both the pixel layer and the service material are shifted. The services are modeled as a separate layer with a material budget of $2\,\%$ that covers the fibre acceptance and is placed at the same z position as the pixel layer (Figure 5). Each pixel layer is given a material budget of $1.74\,\%$ and the momentum resolution for different shifts of the first pixel layer (by $-300\,\mathrm{mm}$, $-500\,\mathrm{mm}$, $-1000\,\mathrm{mm}$) is determined from a toy simulation of 30k events.

The resulting momentum resolution distributions for long tracks are shown in Figure 6, for TTracks in Figure 7. Similarly to what was noted in the modified Run 3 simulation study, only a slight improvement in the momentum resolution for long tracks, predominantly at higher momenta, is observed for larger shifts in the upstream direction. In the

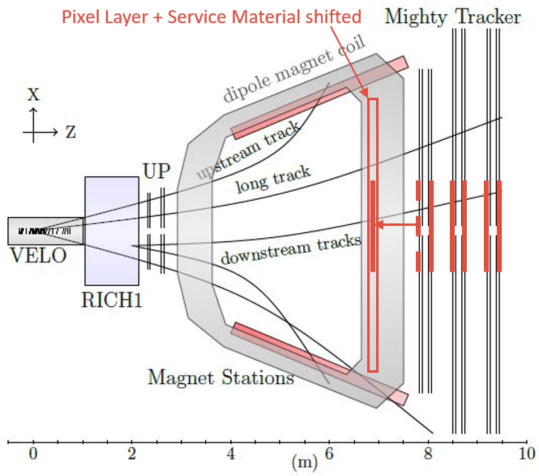

Figure 5: Visualization of shifting the 1st Mighty Pixel layer and service material into the magnet. Adapted from [1].

Table 3: Material budget of the pixel layer and the service material.

	Pixel layer	Service Material
Material Budget x/x_0	$1.74\,\%$	$2\,\%$

low momentum region, the displayed behaviour differs as in this study no worsening of the resolution for very small momenta is seen. This discrepancy is to be attributed to limitations of the parametric description in the framework, such as the assumption of an ideal reference trajectory for the calculation of the resolution. Overall, the shifted configuration gives a momentum resolution in good agreement with the target values of 0.4-$0.5\,\%$.

For TTracks, where the achievable momentum resolution in comparison to long tracks is limited by virtue of the detector setup, the sizeable improvement in the resolution for larger shifts in the upstream direction is confirmed. The larger the shift towards the magnet, the better the momentum resolution as the measurements cover a larger z region which in turn corresponds to an increase in the integrated B field. This observation of resolution improvement for TTracks might be relevant for the search for long-lived particles, which are expected to mostly leave hits in the downstream region.

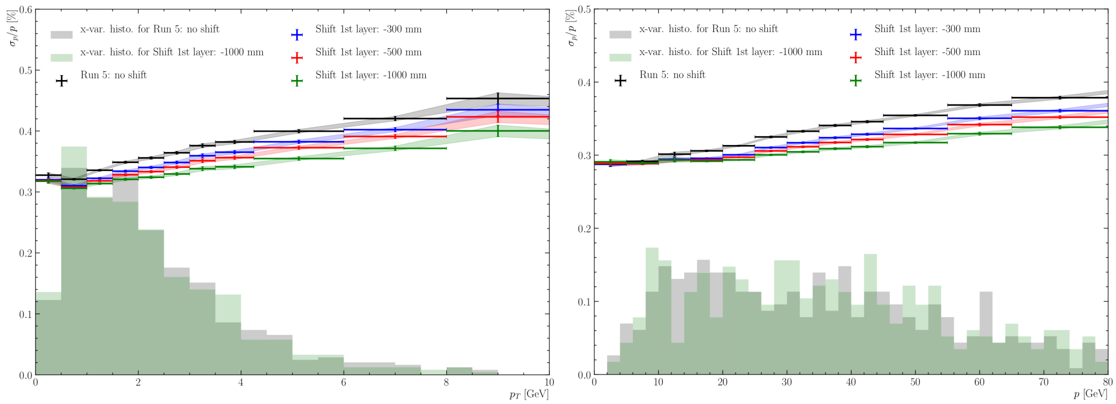

(a) Momentum resolution vs. transverse momentum

(b) Momentum resolution vs. momentum

Figure 6: Comparison of long track momentum resolution for different shifts of the 1st MP layer as a function of kinematic variables. The momentum resolution is displayed for long tracks with hits in the pixel part of the Mighty Tracker.

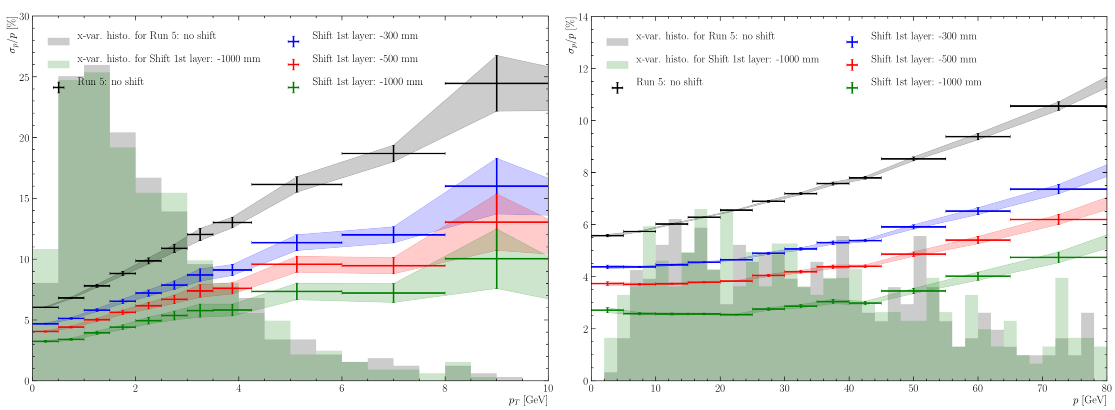

(a) Momentum resolution vs. transverse momentum

(b) Momentum resolution vs. momentum

Figure 7: Comparison of TTrack momentum resolution for different shifts of the 1st MP layer as a function of kinematic variables. The momentum resolution is displayed for TTracks with hits in the pixel part of the Mighty Tracker.

4 Tracking Efficiency Studies

For the first time, a full-acceptance MT reconstruction has been performed running over an Upgrade II simulation. All studies were carried out in the Pattern Recognition Framework.

4.1 Pattern Recognition Framework

The pattern recognition framework is a python-based offline reconstruction tool with custom hit digitization. It uses simulated events and predefined detector geometry masks as input, thereby allowing for the flexible study of the tracking performance with different detector layouts.
In the first step, a Boole-like ([5]) digitization process, the simulated hits are processed according to the hit efficiency, pitch size, and time resolution of the corresponding detector. During the digitization, hits are removed from the detector according to an effective clustering efficiency of 0.98 for the FT and 0.96 for the MT. Additionally, the pitch size is emulated by applying a Gaussian smearing to the position of the hits. Hits are smeared by a width of $\frac{\text{pitch size}}{\sqrt{12}}$. The stand-alone pattern recognition algorithms then reconstruct tracks using these digitized hits. The implemented algorithms include a cheated VELO reconstruction algorithm, with an assumed reconstruction efficiency of $\sim 100\,\%$, and three reconstruction algorithms to reconstruct the full acceptance of the MT. Provided that both the Velo and the TTrack reconstruction algorithms are executed, long tracks can be formed by matching Velo and MT track segments. Lastly, to evaluate the performance of the respective pattern recognition algorithm, a PrChecker (performance checker) is run over the reconstructed tracks.

4.2 Simulation

All results for the full Mighty Tracker reconstruction discussed in this study are obtained using a minimum bias sample simulated over the Upgrade II detector layout. The sample has a luminosity working point of $\mathcal{L} = 1.5 \times 10^{34}\,\mathrm{cm}^{-2}\,\mathrm{s}^{-1}$ and does not include spillover effects. Spillover refers to hits from prior or next bunch crossings that still populate the detector. Running the reconstruction at this luminosity without the inclusion of spillover provides safety margins in the tracking performance for the more likely luminosity of $1.0\text{-}1.3 \times 10^{34}\,\mathrm{cm}^{-2}\,\mathrm{s}^{-1}$ with spillover for the baseline scenario.

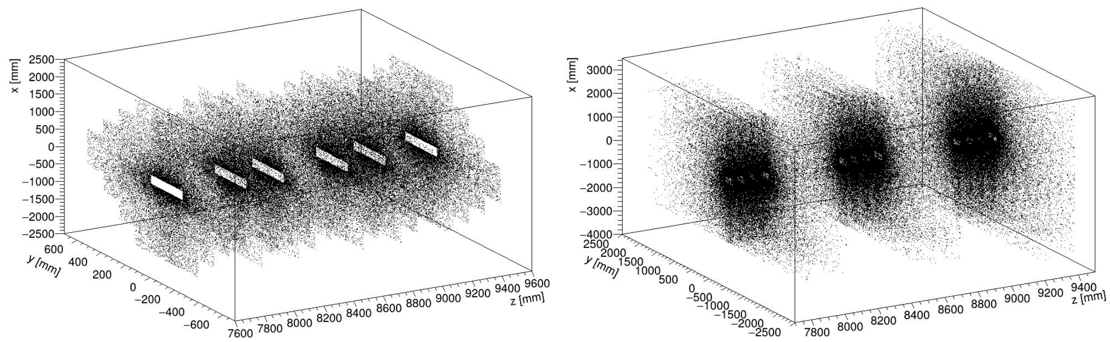

(a) MP acceptance

(b) full FT acceptance

Figure 8: Mighty Pixel acceptance (left) and full Fibre Tracker acceptance (right) in the utilized Upgrade II simulation.

As the simulation includes both the full Fibre Tracker acceptance (Figure 8(b)) as well as the Mighty Pixel acceptance (Figure 8(a)) at a different z position to the FT, the sample can be used to study the tracking performance for both the default and shifted setup (see Section 2.3.2) for the Mighty Tracker.

For the shifted setup scenario, hits in the pixel region of the tracker are taken from the MP acceptance. All hits populating the pixel region in the full FT acceptance are removed and the remaining hits are used as fibre hits. In contrast, solely hits in the full FT acceptance are used for building the default setup scenario. Hits in the pixel region are not cut but instead are treated as pixel hits in the custom hit digitization process, while all other hits are again used as fibre hits.

The size of the pixel region in the two scenarios is dependent on the geometry mask (`Baseline`, `Low`, `Medium`, `High`) applied to the simulation.

4.3 Reconstruction Performance Metrics

The two metrics for testing the track reconstruction performance of the pattern recognition algorithms used throughout this study are the *track reconstruction efficiency* and the *ghost rate*. The track reconstruction efficiency is defined as

$$\varepsilon = \frac{N_{\text{reconstructed\&MC-matched}}}{N_{\text{reconstructible}}}, \tag{4.1}$$

where $N_{\text{reconstructible}}$ gives the number of reconstructible tracks and $N_{\text{reconstructed\&MC-matched}}$ the number of tracks that were reconstructed and subsequently successfully *truth-matched*. A track is considered truth or MC-matched, when at minimum $70\,\%$ of the hits on the track can be attributed to the same particle. The number of reconstructible tracks is determined by how many particles pass the requirements of having left a minimal amount of hits in each of the different tracking subdetectors. These requirements are dependent on the type of track studied. In order for a track to be defined as a long reconstructible in this study, the simulated particle has to leave three hits in the VELO, two in the UP and three x and y information from the MT are needed. This requires either a hit in the pixel region or one hit in a x and a stereo layer of the scintillating fibre detector for each of the three T stations of the MT.
A track is referred to as a ghost track, if less than $70\,\%$ of its hits can be associated to the same particle. The ghost rate is then given as

$$r_{\text{ghost}} = \frac{N_{\text{ghost}}}{N_{\text{reconstructed}}}. \tag{4.2}$$

Here, N_{ghost} is the number of tracks that failed the truth-matching, while $N_{\text{reconstructed}}$ is the number of tracks that were reconstructed by the tracking algorithm.
Due to the emission of bremsstrahlung by electrons and the thus increased difficulty in the track reconstruction, the efficiencies given throughout this study exclude tracks with electron contributions.

4.4 TTrack Reconstruction

TTracks are reconstructed using solely hits from the Mighty Tracker. Since only fringe magnetic fields extend into the MT, only a limited momentum resolution can be achieved (see Section 3.3). Nevertheless, the reconstruction of these tracks is crucial for long track reconstruction, as TTracks can serve as seeds for long tracks. Due to the hybrid nature of the tracker, three different track types, displayed in Figure 9, can be identified, each requiring its own separate reconstruction algorithm.

The nomenclature **Pixel-to-Pixel** tracks refers to tracks traversing only the pixel region of the MT. The reconstruction algorithm starts with forming a two-hit combination using a hit in a pixel layer from the first T station and a pixel layer hit from the last T station. Additional hits in previously unused pixel layers are then collected, provided

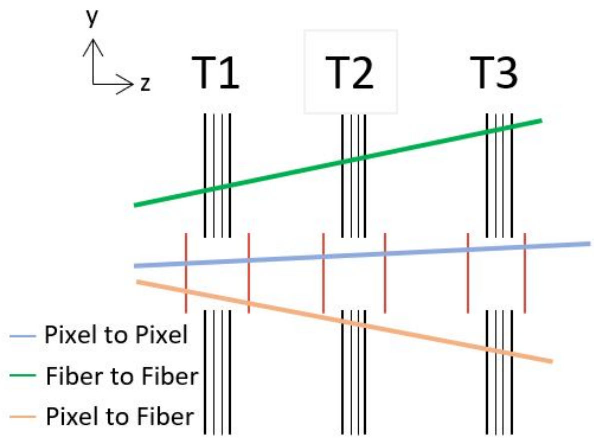

Figure 9: Sketch of the three different TTrack types.

that they are found within a pre-defined search window around a straight line extrapolated from the first two hits. Extrapolating via a straight line is sufficient as tracks reconstructed by this algorithm are mostly high momentum tracks. At least two further hits besides the hits used in the two-hit combination are needed. Thus, a minimum of four hits is required for track reconstruction. One of the additional hits has to stem from the second T station, the other from either the first or the last T station. As TTrack model (Equation (4.3)), a third-order polynomial is fit to the collected hits, and the track with the best fit quality is kept. If the three-hit finding routine is included, track reconstruction is possible requiring only a minimum of three hits in the pixel layers.

Fibre-to-Fibre tracks are tracks leaving hits only in the FT. The **Fibre-to-Fibre** reconstruction algorithm implemented in the offline pattern recognition framework is largely based on the *Hybrid Seeding* algorithm currently utilized in Run 3 as described in [6]. For incorporation in the offline tool, changes have been made to the inclusion of stereo layer hits, which while slightly reducing the track reconstruction efficiency in comparison to the efficiencies achieved with the implementation within the LHCb framework, render the algorithm more time efficient.

Migrating or **Pixel-to-Fibre** tracks are defined as tracks originally starting in the pixel region and ending in the fibre acceptance.
The main focus of this study is on the adaptation and evaluation of the prior implemented Pixel-Fibre reconstruction algorithm for the shifted setup described in Section 2.3.1 as well as for the different geometries described in Section 2.3.1, as changing the detector layout from the default to the shifted scenario mainly affected the reconstruction of

the migrating tracks. The reconstruction algorithm is explained in detail in Section 4.5.1.

4.4.1 Hit Flagging

To reduce combinatorics, the Pixel-to-Pixel algorithm is executed first and all hits found to be a part of a pixel-to-pixel track are flagged. These flagged hits are then not taken into consideration for the other algorithms thereby improving the ghost rate and the needed computation time. Flagging hits without negatively impacting the reconstruction performance of the other track reconstruction algorithms is possible due to the high efficiency and very small ghost rate of the Pixel-to-Pixel algorithm.

4.5 Reconstructing Migrating Tracks

Depending on the chosen pixel geometry, migrating tracks contribute $\sim 10\,\%$ to long reconstructible tracks and $\sim 15\,\%$ to TTracks. For a full breakdown of the contributions for the different geometries and setups, see Appendix A. While the reconstruction of these tracks can be considered more complex, for reaching a high overall reconstruction efficiency for the full MT acceptance, this is a non-negligible amount of tracks. Additionally, the reconstruction of these tracks and the reconstruction performance have an influence on internal alignment considerations as well as overlap studies between pixel and fibre modules.

4.5.1 The Pixel-to-Fibre Algorithm

The Pixel-to-Fibre algorithm described here is an adaptation of a previously implemented algorithm outlined in [7]. Changes were made to the logic to ensure a good performance of the algorithm on the shifted setup scenario. To tune the algorithm, truth tracks from the simulation are used. Electron tracks are not considered in this study. Only long reconstructible tracks, e.g. tracks considered reconstructible in both VELO and MT and stemming from the primary vertex or the decay of a b or c hadron, are taken into account.

The structure of the algorithm is shown in Figure 10. The algorithm is first divided into four cases depending on the combination of x layers in the T1 and T3 stations to account for hit inefficiencies.

Table 4: Two- and three-hit combinations depending on the case. The two-hit combination defining a case is given by the combination of pixel x layers in the T1 with fibre x layers in the T3 station and is the same for both subcases. The subcases are defined by the layers in the T1, T3, and T2 stations forming a three-hit combination.

	Case 0		Case 1		Case 2		Case 3	
	0.1	0.2	1.1	1.2	2.1	2.2	3.1	3.2
T1 station: Pixel layer	$1x$	$1x$	$2x$	$2x$	$1x$	$1x$	$2x$	$2x$
T3 station: Fibre layer	$2x$	$2x$	$2x$	$2x$	$1x$	$1x$	$1x$	$1x$
T2 station	$1x$	$2x$	$1x$	$2x$	$1x$	$2x$	$1x$	$2x$

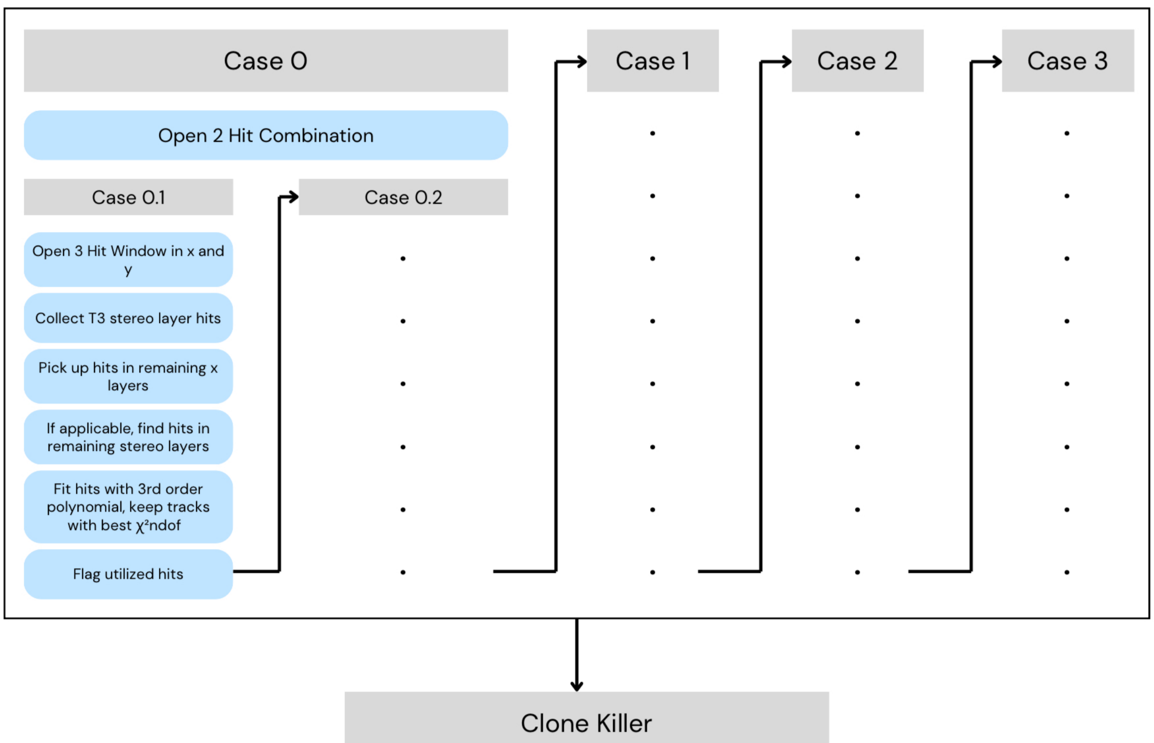

Figure 10: Structure of the Pixel-to-Fibre algorithm. The algorithm is divided into four cases according to the combination of x layers in the T1 and T3 stations. The x layer in the T1 station has to belong to a pixel module, while the x layer in T3 is required to be a fibre layer. Each case is further divided into two separate cases depending on which T2 x layer is added to form the three-hit combination. Besides the two-hit and three-hit combination, the algorithm consists of four main steps: the collection of hits in the stereo layers of the T3 station, the pick up of hits in the remaining x layers, the track fit, and the hit flagging. The addition of possible hits in the T1 and T2 stereo layers is an intermediate step only executed if the T1 or the T2 x layers contain fibre hits. After each case has been executed, a clone killer is applied to the fitted tracks.

For reconstructing migrating tracks, the Pixel-to-Fibre algorithm focuses on tracks that start in the MP and end in the FT. Thus, the hits in the x layer in T1 are required to be in the pixel acceptance, while the hits in the x layer in T3 have to be in the fibre acceptance. Each case consists of two further cases to cover the addition of an x layer from the T2 station. The combination of layers belonging to a case is listed in Table 4. An overview of the steps for each case can be found in Figure 11.

1. **Two-Hit Combination:** Two-hit combinations are formed from a hit in a pixel x layer of T1 and a hit in a fibre x layer of T3. Given a hit in the T1 layer, hits in the T3 layer lying in the tolerance around the predicted hit position in T3 are collected (see Figure 11(a)). To predict the x value of the hit in T3, a straight line is assumed in the bending plane. This parametrization for the two-hit combination can be chosen since only a small magnetic field extends into the MT. The parameters for the straight line are determined on truth tracks from the fit to the 2D distribution of the x coordinate in T3 vs the x coordinate in T1 and vary from case to case. Depending on the case, different x layers are used to form the two-hit combination.
2. **Three-Hit Combination:** A third hit is added to the two-hit combination from one of the T2 x layers, thus creating a three-hit combination. The choice of the T2 layer is dependent on the executed subcase. For extrapolating into the T2 x layer, the y-z projection track is assumed to have originated at $y_{\text{orig}} = 0\,\text{mm}$ and $z_{\text{orig}} = 0\,\text{mm}$. In the bending plane, the x-z-plane, the T2 x_{pred} value is predicted from the slope of the straight line between the two hits in T1 and T3. Since hits in the fibre x layers do not contain y information, the y_{pred} value in T2 is calculated from the slope of the line connecting the origin with the pixel hit in T1. All hits within a given tolerance around the predicted values are retrieved. If the predicted positions correspond to a position in a fibre layer, no requirement for the y position is used. Before hit collection, a correction is applied to the predicted x_{pred} values to correct for the effect of the magnetic fringe fields. The corrections are derived from truth tracks and have been determined separately for the Baseline and the Low geometry of the shifted setup. The application of these corrections permits the use of tight search windows which decreases combinatorics thereby reducing the ghost rate and the computation time. After the creation of the three-hit combination, a parabolic track model is fit to the hits in the bending plane.

   While implementing the shifted setup, the hit collection in this step had to be modified. Shifting the pixel modules out of the fibre layers allows for a particle to leave hits both in the pixel and fibre part, as illustrated in Figure 11(b). To collect both fibre and pixel hits, the fibre and pixel x layer acceptances cannot be treated as a unique layer anymore. Hence, the algorithm now calculates the predicted (x, y) values for pixel and fibre layers separately, taking the different z positions into account.

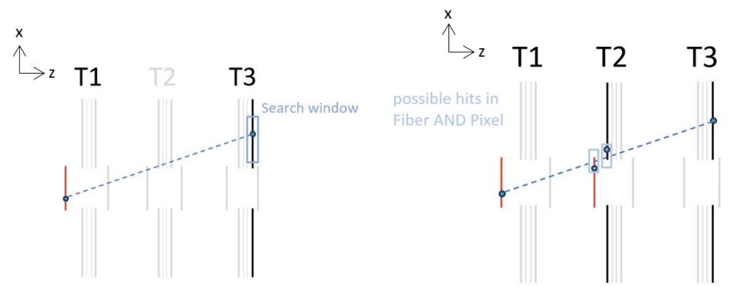

(a) 1st step: Two-hit combination.

(b) 2nd step: Three-hit combination.

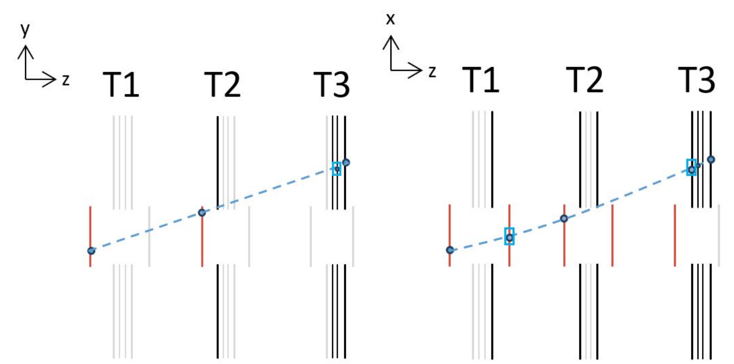

(c) 3rd step: T3 stereo hit collection.

(d) 4th step: Pick up hits in x layers.

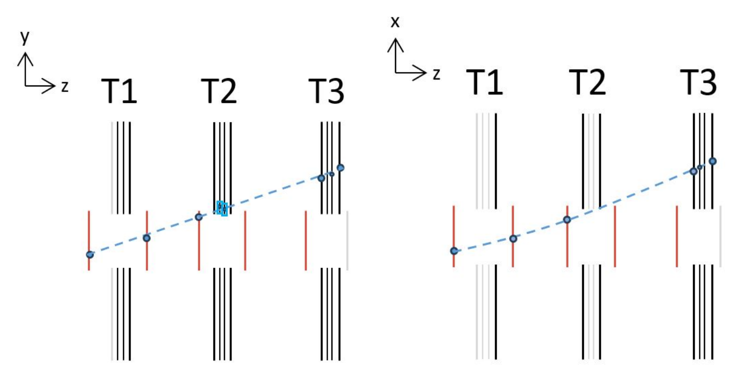

(e) 5th step: T1 and T2 stereo hit collection.

(f) Final step: Track Fit.

Figure 11: Visualization of the different steps of the Pixel-to-Fibre algorithm.

3. **T3 Stereo Hit Collection:** The third step deals with the collection of hits in the stereo layers of T3 in order to obtain y information for the more precise description of the track in the y-z-plane. The y value of the u/v hits is calculated by combining the hits in u/v with the predicted x_{pred} value for the respective layer. In turn, x_{pred} is determined by extrapolating the parabola fit to the three-hit combination into the stereo layers. Depending on whether the hit in the T2 x layer was found in the pixel acceptance or not, the y_{pred} value is computed using an updated line connecting the T1 pixel hit to the T2 pixel hit or using the line connecting the origin of the track to the T1 pixel hit. The inclusion of a possible pixel hit also affects the tolerances around the track, since the opened search window can then cover a smaller region due to the more precise prediction (Figure 11(c)). With the additional y information provided by collecting the stereo hits in T3, the linear fit describing the track in the y-z plane is updated.
4. **x Layer Hit Collection:** After updating the y-z track projection, additional hits are searched for in the three remaining unused x layers distributed over the T1, T2, and T3 stations. For each x layer, the x coordinate x_{pred} is predicted by calculating the x position at the respective z position of the layer from the parabolic track model fit with the three-hit combination. Similarly, the y coordinate y_{pred} is determined from the updated y-z fit. Again, search windows, smaller in x, wider in y, around the predicted values are opened and all hits within the tolerances are collected. A preliminary track fit combining both x-z and y-z model is then performed before continuing with the stereo hit addition, if applicable, and the final track fit.

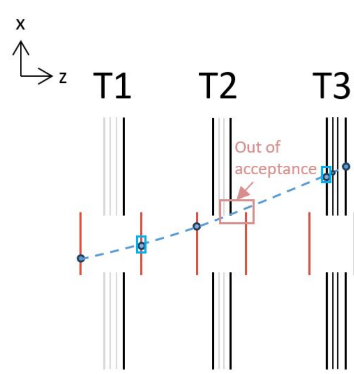

Figure 12: Sketch of the fourth step of the Pixel-to-Fibre algorithm. The change in track reconstruction due to the implementation of the shifted setup is highlighted.

The amount of x layers required to have hits contributing to a track has a major effect on the performance of the track reconstruction algorithm for the shifted setup. Due to the shift of the pixel layers, a particle can traverse the z region of a T station's x layer without leaving a hit in either the pixel or the fibre layer (Figure 12). Requiring a hit in every of the six x layers of the T stations, as was done for the default setup, would therefore lead to a degradation of performance for the shifted setup. Hence, the criteria that a track has five hits distributed over all x layers is chosen as a minimal requirement for track reconstruction.

5. **Stereo Hit Collection:** This is an intermediate step only executed for tracks where the T1 or T2 x layer hits were found in the fibre acceptance. If all collected T1 and T2 hits in a track are pixel hits, no stereo hit search will be carried out since the track does not cross the acceptance covered by the stereo layers. Similar to the procedure outlined in the T3 Stereo Hit Collection step, the y information of the stereo hits is calculated from the x_{pred} value and the respective u/v hits. The x_{pred} value is obtained by evaluating the x-z track projection that includes all hits in x layers at the respective z positions of the stereo layers. A small search window is opened around the y_{pred} value, calculated by the evaluation of the track in the y-z plane at the respective z positions, and all hits satisfying the search window requirement are collected (Figure 11(e)).
6. **Final Track Fit:** The final track fit is performed after all hits have been collected. Using a χ^2 minimization, the system of linear equations arising from the parametrizations of the track in the x-z plane and y-z plane is solved. In the x-z plane, the trajectory of a particle is described by a third-degree polynomial to account for the effect of the magnetic field on the particle:

$$x(z) = x_0 + b_x \cdot (z - z_0) + c_x \cdot (z - z_0)^2 \cdot (1 + \texttt{dRatio} \cdot (z - z_0)^3), \tag{4.3}$$

where x_0 is the x position at a given reference position z_0 and `dRatio` is a fixed, approximately constant parameter that includes the dependency of the magnetic field in y direction on z. [8]

Due to the negligibly small magnetic field in x-direction, the track in the y-z plane can be described by a simple linear fit model:

$$y(z) = y_0 + b_y \cdot (z - z_0) \tag{4.4}$$

y_0 gives the y coordinate at the reference position z_0.

Depending on whether the stereo hit collection step was executed, different selection criteria are applied to the final track fit. If a track contains no hits in the stereo layers of T1 and T2, the track candidate is accepted as a track for a $\chi^2_{\text{ndof}} < 15$. For tracks with hits in these stereo hits, a tighter selection requirement of $\chi^2_{\text{ndof}} < 5$ is applied (Figure 11(f)).

7. **Hit Flagging:** The hits utilized in the final tracks found by the subcase are flagged and removed from consideration for the following cases thus reducing the available combinatorics for the following cases.

After fitting all track candidates, a clone killer is applied to the surviving candidates. The clone killer compares two tracks that are deemed close to one another and, if the tracks have a $20\,\%$ overlap in either pixel or fibre hits, selects the best track based on the number of hits on the track as well as the χ^2_{ndof} of the fit.

4.6 TTrack Reconstruction Performance

Using the metrics defined in Section 4.3, the performance for all three TTrack reconstruction algorithms is evaluated on the simulated Upgrade II sample described in Section 4.2. For every algorithm, the reconstruction efficiencies are calculated for all four geometries (Section 2.3.1) and the two different setups (Section 2.3.2). The efficiencies are given for non-electron tracks in the full acceptance of the spectrometer ($2 < \eta < 5$) covering a momentum region of $p > 5\,\text{GeV}$.

4.6.1 Performance on the Baseline Geometry

This section only presents the performance numbers for the Baseline geometry for both shifted and default setups without the three-hit finding routine of the Pixel-to-Pixel algorithm enabled. A list of all performance numbers for the different geometries and setups as well as with and without the three-hit finding routine for the PixPix algorithm is given in Appendix B.

The efficiencies and ghost rates for the different TTrack reconstruction algorithms are presented in Table 5. The ghost rates are evaluated for the respective track containers separately. In Figure 13 and Figure 14, the reconstruction efficiency in dependence on the momentum as well as the ghost rate depending on the number of reconstructed hits

Table 5: Efficiencies evaluated on the Baseline geometry for both default and shifted setup. The reconstruction performance is given for every TTrack reconstruction algorithm as well as the overall performance, with the performance numbers of the Pixel-to-Fibre algorithm highlighted. The three-hit finding routine for the Pixel-to-Pixel algorithm is not enabled.

Setup	Metric	PixPix [%]	FibFib [%]	**PixFib [%]**	Overall [%]
Default	Efficiency ε	97.11	92.21	**89.76**	95.56
	Ghost Rate	0.15	7.08	**25.11**	5.51
Shifted	Efficiency ε	97.48	92.56	**91.87**	96.10
	Ghost Rate	0.15	6.95	**21.72**	5.15

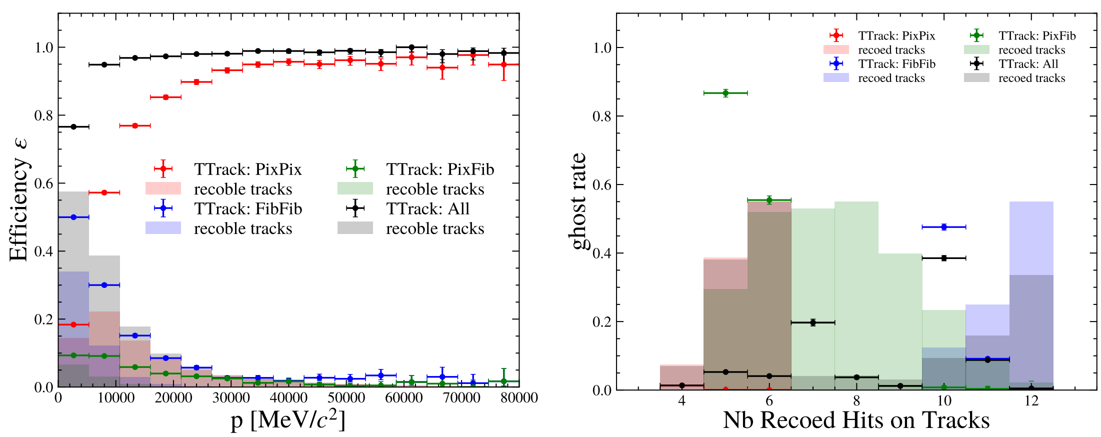

(a) Efficiency vs. momentum (b) Ghost Rate vs. nb of recoed hits on track

Figure 13: Track reconstruction efficiency and ghost rate for the shifted setup and the Baseline geometry in dependence of momentum and the number of reconstructed hits on a track, respectively.

on a track are plotted for the shifted and default setup, respectively.

In the low momentum region, a drop in efficiency is visible which can be attributed to low momenta tracks being subject to more multiple scattering as well as the larger curvature of the tracks which requires the opening of larger search windows, thus increasing the combinatorics and the likelihood of choosing the wrong combination. Tracks in this momentum region are mostly reconstructed using fiber hits, while tracks with higher momentum tend to traverse only the pixel acceptance due to the smaller track curvature. Comparing the performance of the Pixel-to-Pixel and the Fibre-to-Fibre algorithm for the default and the shifted setup, no significant difference in the results is seen. The Pixel-to-Pixel algorithm has a very high efficiency of $\sim 97\,\%$ with a very low ghost rate of $0.15\,\%$ for both setups. At the cost of a higher ghost rate of $\sim 2\,\%$, the reconstruction efficiency can be improved to $\sim 98\,\%$ by the inclusion of the three-hit finding routine. Similar to the Pixel-to-Pixel algorithm, the performance numbers of the Fibre-to-Fibre algorithm remain largely unchanged. This was to be expected since the number of reconstructible tracks in the fibre acceptance remains largely unaffected by the shift in z of the pixel layers.

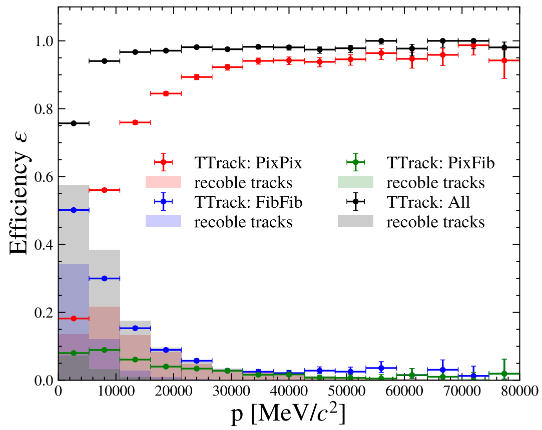

(a) Efficiency vs. momentum

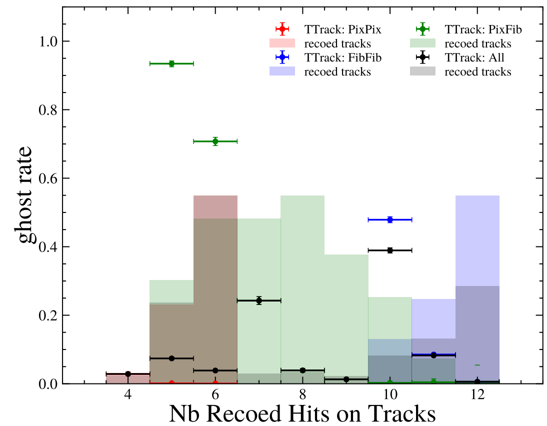

(b) Ghost Rate vs. nb of recoed hits on track

Figure 14: Track reconstruction efficiency and ghost rate for the default setup and the Baseline geometry in dependence of momentum and the number of reconstructed hits on a track, respectively.

Conversely, the switch to the shifted setup had an impact on the performance of the Pixel-to-Fibre algorithm necessitating the modification of the logic of the algorithm as outlined in Section 4.5.1. With the modified algorithm, a slight gain in efficiency and an improvement in the ghost rate are observed. Still, the ghost rate for this algorithm exceeds the ghost rate of the other algorithms (see Figure 13(b)). Due to the comparatively small amount of tracks, however, the ghost rate of this track container does not drive the overall ghost rate. Overall, all three algorithms modified for the shifted setup perform well in terms of both reconstruction efficiency and ghost rate, with the performance being on par or even slightly exceeding the performance for the default setup.

4.6.2 Performance on different Pixel Geometries

The performance of the TTrack reconstruction algorithms on the shifted setup scenario has further been tested with all four Mighty Pixel geometries. The overall track reconstruction efficiencies and ghost rates are displayed in Table 6 and Figure 15.

Comparing the overall efficiencies for all scenarios shows that the efficiencies remain stable at $\sim 94 - 96\,\%$ for all geometries. Thus, no significant changes in the efficiency distribution in dependence on the momentum can be observed (Figure 15(a)).

Table 6: Overall efficiencies evaluated on the shifted setup for the Baseline, Low, Medium, and High geometry. The performance numbers are given without the inclusion of the three-hit finding routine in the Pixel-to-Pixel algorithm.

Geometry	`Baseline` [%]	`Low` [%]	`Medium` [%]	`High` [%]
Efficiency ε	96.10	94.01	95.66	95.70
Ghost Rate	5.15	31.65	12.44	12.72

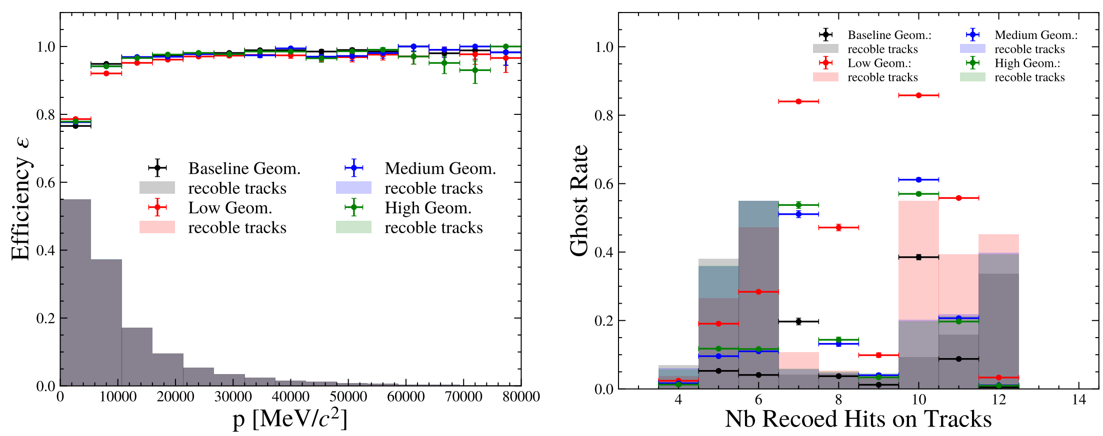

(a) Efficiency vs. momentum

(b) Ghost Rate vs. nb of recoed hits on track

Figure 15: Overall Track reconstruction efficiency and ghost rate evaluated on the shifted setup for all geometries in dependence of momentum and the number of reconstructed hits on a track, respectively.

However, the robustness of the algorithms with regard to the size of the pixel module comes at the cost of increasing ghost rates for smaller pixel module sizes. Most prominently, this is seen for the Low geometry, which has the lowest efficiency with $94\,\%$, but the highest ghost rate with $\sim 31\,\%$. For comparison, the Baseline geometry, which performs best in both metrics and has the largest pixel acceptance, has an efficiency of $96\,\%$ and a ghost rate of $\sim 5\,\%$.

The increase in ghost rate for smaller pixel acceptances is largely driven by the higher occupancy in the fibers as can be seen in Figure 15(b). For larger numbers of reconstructed hits on a track, the ghost rate is very high. Larger numbers of recoed hits on a track, especially in the region of 10-12 hits, correspond to tracks reconstructed by the Fibre-to-Fibre algorithm, while a small amount of recoed hits on a track (4-6 hits) corresponds to tracks reconstructed by the Pixel-to-Pixel algorithm. Thus, the ghost rate is the highest for the Low geometry as it has the largest fiber acceptance. Better ghost rates could potentially be achieved by tuning the algorithms for every geometry, however, this would most likely also result in a drop in efficiency.

5 Long Track Reconstruction via Matching

To reconstruct long tracks, essential for physics analysis also due to their excellent momentum resolution, a pre-existing algorithm known as "matching" is used in the offline framework.

The algorithm creates long tracks using cheated, e.g. truth-matched, VELO track segments as well as reconstructed MT tracks by matching every VELO to every TTrack. Obvious fake matches are rejected by predicting the track state parameters at the exit of the VELO from the TTrack state parameter in the middle of the MT and then discarding any matches where the predicted state parameters differ more than a predefined tolerance from the actual state parameters. Using XGBoost, a BDT is trained on variables including, but not limited to, the track state parameters at the exit of the VELO and the middle of the MT as well as a χ^2 emulating metric ([9]) measuring the quality of a match and then applied on the found combinations. For every TTrack type, a separate BDT is trained. Lastly, combinations are rejected as matches if the predicted classifier output of the match does not pass the specified BDT output cut.

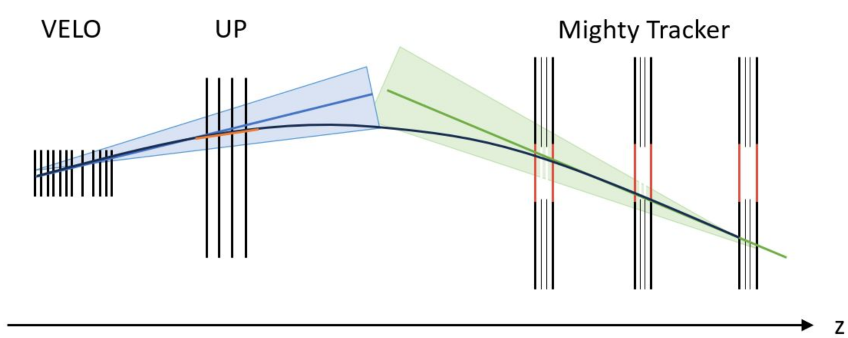

Figure 16: Reconstructing long tracks using the matching algorithm. The algorithm takes track segments from the VELO detector and tracks reconstructed in the MT as the input. The matching plane is at $z = 770\,\mathrm{mm}$ (exit of the VELO) and the match quality is evaluated by a BDT.

In Table 7, the overall track reconstruction efficiencies and ghost rates as well as split according to the TTrack type are given. They are obtained on the shifted setup using the pre-existing matching algorithm. High matching efficiencies of $\sim 90\,\%$ are observed, however, the ghost rates are also quite elevated with an overall ghost rate of $\sim 75\,\%$. The high overall ghost rate is driven by the tracks ending in the high occupancy region and being reconstructed via pixel hits. These are mainly high momentum tracks with little to no curvature, thus it is more difficult to pick the correct match from the high level of combinatorics with straight track segments. Hence, the ghost rate tends even higher to $\sim 80\,\%$.

While retraining the BDTs as well as tighter classifier outputs lead to an improvement in the ghost rate, also significant drops in efficiency, especially for the tracks traversing only the pixel acceptance are seen.

BDTs	Metrics	PixPix [%]	FibFib [%]	PixFib [%]	Overall [%]
Pre-existing	Efficiency ε	93.42	87.62	91.18	91.68
	Ghost Rate	81.56	56.45	52.04	75.99
Retrained	Efficiency ε	90.17	89.18	88.24	87.72
	Ghost Rate	75.70	34.07	35.52	66.36

Table 7: Performance of the original and the retrained BDT for long tracks found via matching. Different cuts on the classifier output for each BDT are applied in the matching process.

Thus, to improve the ghost rate while maintaining a high reconstruction efficiency, the inclusion of hits from the UP is proven to be crucial for the long track reconstruction performance.

As of now, no algorithm or parametrization is in place to incorporate the correct UP hits into the matching algorithm. An approach to collect UP hits is to predict the parameters for the local UP track model given the VELO and MT track state parameters for a match. The UP hits can then be selected according to the best χ^2 matching criterion. However, further work is required here.

6 Conclusion

For the proposed Upgrade II, where a substantial increase in luminosity entails challenges for detector and tracking such as high pile-up and high occupancy, existing tracking algorithms have to be revisited and new tracking algorithms have to be developed to provide a robust tracking performance in the new physics environment. The aim of the work presented here has been the study of the impact of different detector designs on the tracking performance. Particular focus has been given to the description and performance of the new stand-alone pattern recognition algorithm for tracks passing through both the fibre and pixel acceptance of the Mighty Tracker, a hybrid detector scheduled to replace the current SciFi detector in Upgrade II.

Two studies on the effect of material placement in the UP as well as the position of the first MightyPixel layer on the momentum resolution for different track types have been carried out. The comparison of the momentum resolution of long tracks for different repartitions of the material in the UP leads to the conclusion that the minimization of the material budget at the exit of the UP could potentially result in a significant improvement in the momentum resolution for long tracks. Similarly, when shifting the first MP layer upstream, and thus increasing the integrated B field, a sizeable improvement in the momentum resolution is seen for TTracks. This result might prove to be relevant in the search for and the reconstruction of long-lived particles and their daughters.

For the first time, a full MT reconstruction over an Upgrade II simulated sample is run in an offline python-based pattern recognition framework. The existing TTrack reconstruction algorithms, modified to take a mechanically feasible MT layout (pixel and fiber layers at different z positions) into account, prove to be robust against changes made to the size of the pixel acceptance of the MT. This, however, comes at the cost of increased ghost rates. Nevertheless, good overall track reconstruction efficiencies of $94 - 96\,\%$ for non-electron high momenta tracks in the acceptance of the detector are obtained.

Further work is still needed in the reconstruction of long tracks from VELO and MT track segments via the matching algorithm. Without hits in the UP, a high long track reconstruction efficiency of $\sim 90\,\%$ is only attained for high ghost rates of $\sim 70\,\%$, particularly in the high-occupancy region. A decrease in the ghost rate without including the UP can only be achieved by accepting a loss in efficiency. Thus, the inclusion of the correct UP hits is crucial for maintaining a high reconstruction efficiency while keeping the ghost rate in check.

List of Figures

List of Tables

References

[1] LHCb Collaboration. *Framework TDR for the LHCb Upgrade II: Opportunities in flavour physics, and beyond, in the HL-LHC era*. Tech. rep. Geneva: CERN, 2021. URL: https://cds.cern.ch/record/2776420.

[2] R. Quagliani. *Upgrade 2 studies, Mini LHCb*. RTA WP6 Meeting. Mar. 23, 2023. URL: https://indico.cern.ch/event/1267323/contributions/5322120/attachments/2616800/4523187/rquaglia_upgrade2Slides_WP6.pdf.

[3] P. Billoir. *Kalman Filter and byproducts - using the weight matrix formalism*. 6th LHCb Computing Workshop. Nov. 18, 2015. URL: https://indico.cern.ch/event/337568/contributions/1733018/attachments/1189146/1725559/Billoir_WeightFormalism.pdf.

[4] C. Langenbruch. *Tracking Performance Studies*. 4th Mighty Tracker Workshop at Liverpool. July 2, 2024. URL: https://indico.cern.ch/event/1403159/contributions/6018302/attachments/2888508/5063077/liverpool_langenbruch.pdf.

[5] LHCb Collaboration. *Doumentation for the LHCb digitization programme Boole*. URL: https://lhcbdoc.web.cern.ch/lhcbdoc/boole/ (visited on 09/12/2024).

[6] S. Aiola et al. "Hybrid seeding: A standalone track reconstruction algorithm for scintillating fibre tracker at LHCb". In: *Computer Physics Communications* 260 (Mar. 2021), p. 107713. ISSN: 0010-4655. DOI: 10.1016/j.cpc.2020.107713. URL: http://dx.doi.org/10.1016/j.cpc.2020.107713.

[7] A. Mathad, R. Quagliani. *Mighty Tracker: Pixel to Fibre track finding algorithm*. LHCb Upgrade II Tracking Workshop. Mar. 7, 2023. URL: https://indico.cern.ch/event/1342873/contributions/5838023/attachments/2814899/4913981/Abhijit_MTPixFib.pdf.

[8] R. Quagliani. "Study of double charm B decays with the LHCb experiment at CERN and track reconstruction for the LHCb upgrade". Presented 06 Oct 2017. U. Paris-Saclay, 2017. URL: https://cds.cern.ch/record/2296404.

[9] R. Quagliani. *Long-Tracking at Upgrade 2*. LHCb Upgrade II Tracking Workshop. Mar. 7, 2024. URL: https://indico.cern.ch/event/1342873/contributions/5838028/attachments/2815327/4914877/rquaglia_trackingworkshop_u2_7March2024.pdf.

A Number of Reconstructible Tracks in MightyTracker

For each geometry, the number of overall reconstructible tracks as well as split in the contributions from the three different TTrack types is given. This is done for both default and shifted setup. All numbers require the track to have an MT reconstructible passing the "medium" trigger requirement.

Table 8: Number of Long Reconstructible Tracks. To classify as Long Reconstructible, the track has to have a reconstructible in the VELO and the MT and stem from a primary vertex or a decay.

Default Setup

Geometry	Nb. Recoble Tracks	Pixel [%]	Fiber [%]	Mixed [%]
Baseline	44810	24523 [54.7 %]	16312 [36.4 %]	3975 [8.9 %]
Low	44760	16808 [37.6 %]	24033 [53.7 %]	3919 [8.8 %]
Medium	44776	22005 [49.1 %]	18968 [42.4 %]	3803 [8.5 %]
High	44786	21850 [48.8 %]	18569 [41.5 %]	4367 [9.8 %]

Shifted Setup

Geometry	Nb. Recoble Tracks	Pixel [%]	Fiber [%]	Mixed [%]
Baseline	44688	24784 [55.5 %]	16310 [36.5 %]	3594 [8.0 %]
Low	44604	17006 [38.1 %]	24008 [53.8 %]	3590 [8.0 %]
Medium	44646	22210 [49.7 %]	18972 [42.5 %]	3464 [7.8 %]
High	44640	22117 [49.5 %]	18566 [41.6 %]	3957 [8.9 %]

Table 9: Number of Reconstructible TTracks.

Default Setup

Geometry	Nb. Recoble Tracks	Pixel [%]	Fiber [%]	Mixed [%]
Baseline	113353	64438 [56.8%]	33169 [29.3%]	15757 [13.9%]
Low	112681	44560 [39.5%]	51459 [45.7%]	16669 [14.8%]
Medium	113126	56676 [50.1%]	39896 [35.3%]	16565 [14.6%]
High	113164	56562 [50.0%]	39377 [34.8%]	17236 [15.2%]

Shifted Setup

Geometry	Nb. Recoble Tracks	Pixel [%]	Fiber [%]	Mixed [%]
Baseline	117218	69573 [59.4%]	33164 [28.3%]	14494 [12.4%]
Low	115981	49067 [42.3%]	51463 [44.4%]	15458 [13.3%]
Medium	116685	61491 [52.7%]	39880 [34.2%]	15326 [13.1%]
High	116817	61518 [52.7%]	39364 [33.7%]	15947 [13.7%]

B MT Reconstruction Performance

B.1 Default Setup

Table 10: Track reconstruction efficiencies and ghost rates split into all three algorithms for all geometries. The efficiencies are given for non-electron tracks exceeding $5\,\mathrm{GeV}$.

Geometry	Metrics	PixPix [%]	FibFib [%]	PixFib [%]	Overall [%]
Baseline	Efficiency ε	97.11	92.21	89.76	95.56
	Ghost Rate	0.15	7.08	25.11	5.51
Low	Efficiency ε	96.94	89.93	91.63	93.70
	Ghost Rate	0.20	36.77	59.57	32.34
Medium	Efficiency ε	96.96	91.69	90.91	95.13
	Ghost Rate	0.19	15.47	40.19	12.82
High	Efficiency ε	97.02	91.90	89.43	95.12
	Ghost Rate	0.20	14.82	40.07	13.02

Table 11: Track reconstruction efficiencies and ghost rates split into all three algorithms for all geometries. The efficiencies are given for non-electron tracks exceeding $5\,\mathrm{GeV}$. The three-hit finding routine for the PixPix algorithm is enabled here.

Geometry	Metrics	PixPix [%]	FibFib [%]	PixFib [%]	Overall [%]
Baseline	Efficiency ε	97.93	92.21	89.76	96.16
	Ghost Rate	2.45	7.08	24.86	6.57
Low	Efficiency ε	97.93	89.81	91.56	94.20
	Ghost Rate	2.90	36.77	60.28	32.57
Medium	Efficiency ε	98.13	91.69	90.91	95.91
	Ghost Rate	2.90	15.47	40.07	13.60
High	Efficiency ε	97.97	91.90	89.38	95.75
	Ghost Rate	2.58	14.82	39.98	13.69

B.2 Shifted Setup

Table 12: Track reconstruction efficiencies and ghost rates split into all three algorithms for all geometries. The efficiencies are given for non-electron tracks exceeding 5 GeV.

Geometry	Metrics	PixPix [%]	FibFib [%]	PixFib [%]	Overall [%]
Baseline	Efficiency ε	97.48	92.56	91.87	96.10
	Ghost Rate	0.15	6.95	21.72	5.15
Low	Efficiency ε	97.36	90.15	90.18	94.01
	Ghost Rate	0.21	36.87	57.72	31.65
Medium	Efficiency ε	97.41	92.26	91.22	95.66
	Ghost Rate	0.17	15.65	36.58	12.44
High	Efficiency ε	97.45	92.25	91.08	95.70
	Ghost Rate	0.14	15.15	37.30	12.72

Table 13: Track reconstruction efficiencies and ghost rates split into all three algorithms for all geometries. The efficiencies are given for non-electron tracks exceeding 5 GeV. The three-hit finding routine for the PixPix algorithm is enabled here.

Geometry	Metrics	PixPix [%]	FibFib [%]	PixFib [%]	Overall [%]
Baseline	Efficiency ε	98.35	92.56	91.93	96.74
	Ghost Rate	1.97	6.95	21.43	5.88
Low	Efficiency ε	98.36	90.15	90.18	94.55
	Ghost Rate	2.66	36.87	57.64	31.68
Medium	Efficiency ε	98.28	92.26	91.28	96.25
	Ghost Rate	2.20	15.65	36.57	12.94
High	Efficiency ε	98.36	92.25	91.08	96.32
	Ghost Rate	2.26	15.15	37.19	13.23

Acknowledgements

I want to express my deepest gratitude to my supervisors, Dr. Renato Quagliani and Dr. Alessandro Scarabotto, not only for providing me with the opportunity to work on this project but also for taking the time to explain the intricacies of the carried-out studies as well as tracking algorithms themselves, thus giving me insight into a fascinating topic I was previously unfamiliar with. Without their expert guidance and support, this work would have been tremendously more difficult, nigh impossible. Also, thank you for the amazing food recommendations - they made a lot of us very happy.

I would also like to thank my office mates: In the now one-and-a-half years we have spent in the same offices and lectures, we stuck together through many challenges, cow encounters, and snack shortages. I am already looking forward to the continuation with "Kiddo" and "Kameradenkuh". Thanks also go to our Michigan and Frankfurt friends for dragging us onto adventures and the delicious cooking sessions.

A big thank you goes to the whole LHCb collaboration, especially our office neighbour, for the warm welcome. Additionally, thanks to the Heidelberg LHCb group for their support before and throughout my stay here, for always welcoming another shadow (other than Kiddo and Kameradenkuh), and for the shared meals.

Special thanks go to my partner, friends, and family for always having my back, be it from here or home.